

O. Barry¹

Department of Mechanical
and Industrial Engineering,
University of Toronto,
Toronto, ON M5S 3G8, Canada
e-mail: oumar.barry@utoronto.ca

J. W. Zu

Department of Mechanical
and Industrial Engineering,
University of Toronto,
Toronto, ON M5S 3G8, Canada

D. C. D. Oguamanam

Department of Mechanical
and Industrial Engineering,
Ryerson University,
Toronto, ON M5B 2K3, Canada

Forced Vibration of Overhead Transmission Line: Analytical and Experimental Investigation

An analytical model of a single line transmission line carrying a Stockbridge damper is developed based on the Euler–Bernoulli beam theory. The conductor is modeled as an axially loaded beam and the messenger is represented as a beam with a tip mass at each end. Experiments are conducted to validate the proposed model. An explicit expression is presented for the damping ratio of the conductor. Numerical examples show that the proposed model is more accurate than the models found in the literature. Parametric studies indicate that the response of the conductor significantly depends on the excitation frequency, the location of the damper, and the damper parameters. [DOI: 10.1115/1.4027578]

Keywords: stockbridge damper, Strouhal frequency, messenger, rated tensile strength, overhead transmission line

1 Introduction

Aeolian vibration of overhead transmission lines, also referred to as conductors, is a major factor that contributes to power outages. This type of vibration is wind-induced and the wind speed ranges between 1 and 7 m/s. The vibration is observed in 3–150 Hz frequency range and has peak-to-peak amplitudes of up to one conductor diameter. Aeolian vibration causes fatigue damage of the point of contact between the conductor and the suspension clamp. This can be reduced or eliminated by minimizing the amplitude of vibration near the clamp. It is commonplace to protect conductors from fatigue failure by attaching Stockbridge dampers near the clamps. The effectiveness of this external damping device is dependent on their position on the conductor, their overall characteristics, and the characteristics of the conductor.

The study of Aeolian vibration of overhead transmission lines abound in the literature. The most commonly used approach is the energy balance method (EBM) [1–4], where the vibration level is evaluated by determining the balance between the energy imparted to the conductor by the wind and the energy dissipated by the conductor (via conductor self-damping) and the added dampers. Another approach for predicting the response of the conductor is based on impedance models [5–7]. The single conductor is usually modeled as a cable, and the Stockbridge damper is represented by a single concentrated force on the conductor. This concentrated force is obtained experimentally.

Other methods employed to study the vibration of transmission lines include matrix transfer by Hardy and Noiseux [8], the statistical method by Noiseux et al. [9], and the approach of multiphysics by Tsui [10]. While the simplicity of the aforementioned methods is a major attraction, their robustness suffers in that the complex nature of the coupled-dynamics is not well reflected. The limitation of the dynamics to only one-way coupling between the conductor and damper, a situation where the dynamics of the damper influence that of the conductor but not the converse, is worthy of further investigation.

Gonçalves et al. [11] employ experiments and theoretical models to better understand the system from the viewpoint of a vortex-induced motion or vibration phenomenon. An attempt at

modeling a two-way coupling scenario was reported in Refs. [12] and [13], where both the conductor and damper were modeled as one unified system in order to account for their two-way coupling. However, the conductor self-damping was ignored and the analysis was based on the finite element method (FEM). The finite element model was rather complicated and computationally intensive. The present study is aimed at addressing these shortcomings by including the conductor self-damping and by presenting an analytical approach that yields exact solutions with minimal complications. Experiments were conducted to determine the conductor self-damping and to validate the analytical model. Parametric studies were performed to investigate the effect of the magnitude and location of the damper on the response. The role of the Strouhal frequency on the vibration response was also examined.

2 Governing Equations

A schematic of the conductor with a damper is shown in Fig. 1. A close-up view of the conductor and damper deformation is depicted in Fig. 2. Following Ref. [14], the equations of motion are given as

$$m_c \ddot{w}_{ci} + E_c I_c w_{ci}'''' - T w_{ci}'' = 0 \quad (1)$$

$$m_m \left(\ddot{w}_{c1}^* + (-1)^{(i+1)} \ddot{w}_{c1}^* L_{mi} + \dot{w}_{mi} \right) + E_m I_m w_{mi}'''' = 0 \quad (2)$$

where w_{m1}^* (w_{m2}^*) is the transverse displacement of the right-end (left-end) counterweight, m_1 (m_2) is the tip mass on the right-hand (left-hand) side; L_{m1} (L_{m2}) is the length of the messenger on the right-hand (left-hand) side; m_c (m_m) is the mass per unit length of the conductor (messenger); m_{m1} (m_{m2}) is the mass of the messenger on the right-hand (left-hand) side; T denotes the conductor tension; and $E_c I_c$ ($E_m I_m$) is the flexural rigidity of the conductor

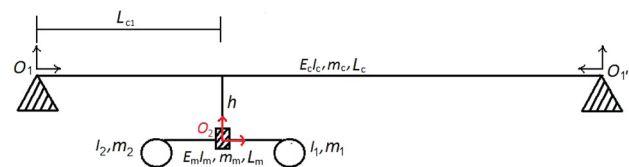


Fig. 1 Schematic of a single conductor with a Stockbridge damper

¹Corresponding author.

Contributed by the Technical Committee on Vibration and Sound of ASME for publication in the JOURNAL OF VIBRATION AND ACOUSTICS. Manuscript received November 9, 2013; final manuscript received April 29, 2014; published online May 22, 2014. Assoc. Editor: Mohammed Daqaq.

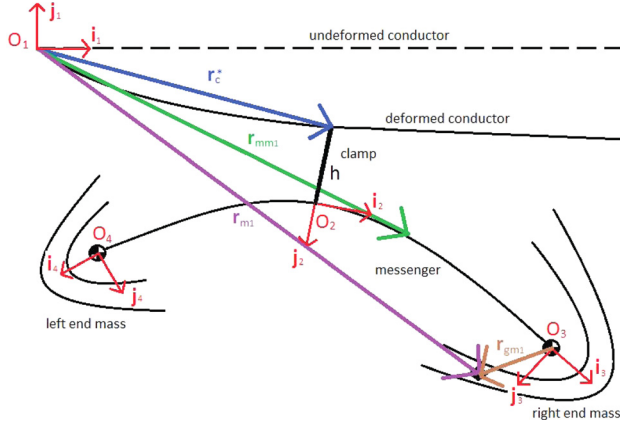


Fig. 2 Close-up of damper

(messenger). The overdots and primes denote temporal and spatial derivation, respectively.

Note that the subscript $i \in \{1, 2\}$ identifies the right-hand and left-hand segments of both the conductor and messenger. The continuity conditions of the displacement at the attachment point of the damper to the conductor, L_{c1} , are written as

$$w_{c1}(L_{c1}, t) = w_{c2}(L_{c2}, t) \quad (3)$$

$$w'_{c1}(L_{c1}, t) = -w'_{c2}(L_{c2}, t) \quad (4)$$

From the variation of the conductor displacement, δw_{c1} , the obtained shear force boundary condition at the location of the damper may be written as

$$\begin{aligned} & \sum_{i=1}^2 \left\{ m_i \left(\ddot{w}_{c1}^* + (-1)^{(i+1)} \ddot{w}'_{c1} L_{mi} + \ddot{w}_{mi}^* \right) + \ddot{w}_{c1}^* m_{mi} \right. \\ & \left. + m_m \int_0^{L_{mi}} \ddot{w}_{mi} dx_m + \frac{1}{2} m_m \ddot{w}'_{c1} (-1)^{(i+1)} L_{mi}^2 \right\} \\ & - E_c I_c \left(w'''_{c1} + w'''_{c2} \right) + T \left(w'_{c1} + w'_{c2} \right) = 0 \end{aligned} \quad (5)$$

The contributions from the tension vanished because of Eq. (4). The bending moment boundary condition at the attachment of the messenger may be expressed as

$$\begin{aligned} & \sum_{i=1}^2 \left\{ m_i \left[(-1)^{(i+1)} \ddot{w}'_{c1} L_{mi} + w_c'^* (h^2 + L_{mi}^2) + (-1)^{(i+1)} L_{mi} \ddot{w}_{mi}^* \right] \right. \\ & \left. + I_i \left(\ddot{w}'_{c1} + (-1)^{(i+1)} \ddot{w}'_{mi} \right) + \ddot{w}'_{c1} h^2 m_{mi} \right. \\ & \left. + m_m \int_0^{L_{mi}} (-1)^{(i+1)} x_m \ddot{w}_{mi} dx_m \right. \\ & \left. + \frac{1}{2} m_m \left((-1)^{(i+1)} \ddot{w}'_{c1} L_{mi}^2 + \frac{2}{3} \ddot{w}'_{c1} L_{mi}^3 \right) \right\} \\ & + E_c I_c \left(w''_{c1} - w''_{c2} \right) = 0 \end{aligned} \quad (6)$$

The last set of boundary conditions for the conductor was obtained by enforcing zero displacement and bending moment at both ends of each segment. This was done to replicate the boundary conditions on a suspension–suspension span

$$w_{ci}(0, t) = 0 \quad (7)$$

$$w''_{ci}(0, t) = 0 \quad (8)$$

With respect to the messenger, the shear force boundary conditions at each end, L_{m1} and L_{m2} , can be expressed as

$$m_i \left(\ddot{w}_{mi}^* + \ddot{w}'_{c1} + (-1)^{(i+1)} L_{mi} \ddot{w}'_{c1} \right) - E_m I_m w'''_{mi} = 0 \quad (9)$$

and the bending moment boundary condition at each end is

$$I_i \left(\ddot{w}'_{mi} + (-1)^{(i+1)} \ddot{w}'_{c1} \right) + E_m I_m w''_{mi} = 0 \quad (10)$$

The Stockbridge damper behaves as a cantilevered beam at the junction of the clamp and the messenger (i.e., $x_m = 0$). Hence, the displacement and rotation of both right- and left-side messenger are zero

$$w_{mi}(0, t) = 0 \quad (11)$$

$$w'_{mi}(0, t) = 0 \quad (12)$$

3 Orthogonality Condition

Following Ref. [14], the orthogonality relation can be expressed as

$$\begin{aligned} & \sum_{i=1}^2 \left\{ m_c \int_0^{L_{ci}} Y_{ci}^{(r)} Y_{ci}^{(s)} dx + m_m \int_0^{L_{mi}} Y_{mi}^{(r)} Y_{mi}^{(s)} dx_m + Y_{c1}^{(r)*} Y_{c1}^{(s)*} (m_i + m_m L_{mi}) \right. \\ & \left. + Y_{c1}^{(r)*} Y_{c1}^{(s)*} \left[m_i (L_{mi}^2 + h^2) + I_i + h^2 m_m L_{mi} + \frac{1}{3} L_{mi}^3 \right] + Y_{mi}^{(r)*} Y_{mi}^{(s)*} m_{mi} + Y_{mi}^{(r)*} Y_{mi}^{(s)*} I_i + (-1)^{(i+1)} m_i L_{mi} \left(Y_{c1}^{(r)*} Y_{c1}^{(s)*} + Y_{c1}^{(r)*} Y_{c1}^{(s)*} \right) \right. \\ & \left. + m_{mi} \left(Y_{c1}^{(r)*} Y_{mi}^{(s)*} + Y_{c1}^{(s)*} Y_{mi}^{(r)*} \right) + m_m \int_0^{L_{mi}} \left(Y_{c1}^{(r)*} Y_{mi}^{(s)*} + Y_{c1}^{(s)*} Y_{mi}^{(r)*} \right) dx_m + (-1)^{(i+1)} \frac{1}{2} m_m L_{mi}^2 \left(Y_{c1}^{(r)*} Y_{c1}^{(s)*} + Y_{c1}^{(s)*} Y_{c1}^{(r)*} \right) \right. \\ & \left. + (-1)^{(i+1)} m_i L_{mi} \left(Y_{c1}^{(r)*} Y_{mi}^{(s)*} + Y_{c1}^{(s)*} Y_{mi}^{(r)*} \right) + (-1)^{(i+1)} I_i \left(Y_{c1}^{(r)*} Y_{mi}^{(s)*} + Y_{c1}^{(s)*} Y_{mi}^{(r)*} \right) \right. \\ & \left. + (-1)^{(i+1)} m_m \int_0^{L_{mi}} x_m \left(Y_{c1}^{(r)*} Y_{mi}^{(s)*} + Y_{c1}^{(s)*} Y_{mi}^{(r)*} \right) dx_m \right\} = \delta_{rs} \end{aligned} \quad (13)$$

where δ_{rs} is the Kronecker delta. Y_{ci} and Y_{mi} are the mode shape of the conductor and messenger, respectively, and their expressions are given in the Appendix.

4 Forced Vibration

The equations of motion for the forced vibration are given as

$$m_c \ddot{w}_{ci} + E_c I_c w_{ci}^{IV} - T w_{ci}'' = F(t) \delta(x - L_c/2) \quad (14)$$

$$m_m \left(\ddot{w}_{mi} + (-1)^{(i+1)} \ddot{w}_{ci}^* x_m + w_{ci}^* \right) + E_m I_m w_{mi}^{IV} = 0 \quad (15)$$

The excitation force is expressed as

$$F(t) = F_0 \sin(2\pi f t) \quad (16)$$

where F_0 denotes the excitation amplitude force in N and f is the forcing frequency in Hz. Using mode superposition principle, the deflection of the beam is assumed as

$$w_{ci} = \sum_{r=1}^{\infty} q_r(t) Y_{ci}^{(r)}(x) \quad (17)$$

$$w_{mi} = \sum_{r=1}^{\infty} q_r(t) Y_{mi}^{(r)}(x) \quad (18)$$

Substituting Eqs. (17) and (18) into Eqs. (14) and (15) yields

$$m_c \sum_{r=1}^{\infty} \ddot{q}_r Y_{ci}^{(r)} + E_c I_c \sum_{r=1}^{\infty} q_r Y_{ci}^{(r)IV} - T \sum_{r=1}^{\infty} q_r Y_{ci}^{(r)''} = F(t) \delta(x - L_c/2) \quad (19)$$

$$m_m \sum_{r=1}^{\infty} \ddot{q}_r \left(Y_{mi}^{(r)} + (-1)^{(i+1)} Y_{ci}^{(r)'} x_m + Y_{ci}^{(r)*} \right) + E_m I_m \sum_{r=1}^{\infty} q_r Y_{mi}^{(r)IV} = 0 \quad (20)$$

Multiply Eqs. (19) and (20) by $Y_{ci}^{(s)}$ and $Y_{mi}^{(s)}$, respectively. An algebraic manipulation of the resulting expressions yields

$$[M_{rs}] \{\ddot{q}_r\} + [K_{rs}] \{q_r\} = [F_r] \quad (21)$$

where

$$\begin{aligned} M_{rs} = & \sum_{i=1}^2 \left\{ m_c \int_0^{L_{ci}} Y_{ci}^{(r)} Y_{ci}^{(s)} dx + m_m \int_0^{L_{mi}} Y_{mi}^{(r)} Y_{mi}^{(s)} dx_m + Y_{mi}^{(r)*} Y_{mi}^{(s)*} m_{mi} + Y_{ci}^{(r)*} Y_{ci}^{(s)*} (m_i + m_m L_{mi}) + m_{mi} \left(Y_{ci}^{(r)*} Y_{mi}^{(s)*} + Y_{ci}^{(s)*} Y_{mi}^{(r)*} \right) \right. \\ & + Y_{ci}^{(r)'} Y_{ci}^{(s)'} \left[m_i (L_{mi}^2 + h^2) + I_i + h^2 m_m L_{mi} + \frac{1}{3} L_{mi}^3 \right] + Y_{mi}^{(r)'} Y_{mi}^{(s)'} I_i + (-1)^{(i+1)} m_i L_{mi} \left(Y_{ci}^{(r)'} Y_{ci}^{(s)*} + Y_{ci}^{(r)*} Y_{ci}^{(s)'} \right) \\ & + m_m \int_0^{L_{mi}} \left(Y_{ci}^{(r)*} Y_{mi}^{(s)*} + Y_{ci}^{(s)*} Y_{mi}^{(r)*} \right) dx_m + (-1)^{(i+1)} I_i \left(Y_{ci}^{(r)'} Y_{mi}^{(s)'} + Y_{ci}^{(s)'} Y_{mi}^{(r)'} \right) + (-1)^{(i+1)} \frac{1}{2} m_m L_{mi}^2 \left(Y_{ci}^{(r)*} Y_{ci}^{(s)'} + Y_{ci}^{(s)*} Y_{ci}^{(r)'} \right) \\ & \left. + (-1)^{(i+1)} m_i L_{mi} \left(Y_{ci}^{(r)'} Y_{mi}^{(s)*} + Y_{ci}^{(s)'} Y_{mi}^{(r)*} \right) + (-1)^{(i+1)} m_m \int_0^{L_{mi}} \left(Y_{ci}^{(r)'} Y_{mi}^{(s)} + Y_{ci}^{(s)'} Y_{mi}^{(r)} \right) dx_m \right\} \end{aligned} \quad (22)$$

$$K_{rs} = \sum_{i=1}^2 \left(E_c I_c \int_0^{L_{ci}} Y_{ci}^{(r)''} Y_{ci}^{(s)''} dx - T \int_0^{L_{ci}} Y_{ci}^{(r)'} Y_{ci}^{(s)'} dx + E_m I_m \int_0^{L_{mi}} Y_{mi}^{(r)''} Y_{mi}^{(s)''} dx \right) \quad (23)$$

$$F_r = F(t) Y_{ci}(x = \frac{L_c}{2}) \quad (24)$$

The orthogonality relation, Eq. (13), is employed to obtain

$$\begin{aligned} M_{rr} = & \sum_{i=1}^2 \left\{ m_c \int_0^{L_{ci}} Y_{ci}^{(r)2} dx + m_m \int_0^{L_{mi}} Y_{mi}^{(r)2} dx_m + Y_{ci}^{(r)*} (m_i + m_m L_{mi}) + Y_{ci}^{(r)2'} \left[m_i (L_{mi}^2 + h^2) + I_i + h^2 m_m L_{mi} + \frac{1}{3} L_{mi}^3 \right] + Y_{mi}^{(r)*} m_{mi} \right. \\ & + Y_{mi}^{(r)2'} I_i + (-1)^{(i+1)} 2 m_i L_{mi} Y_{ci}^{(r)'} Y_{ci}^{(r)*} + 2 m_{mi} Y_{ci}^{(r)*} Y_{mi}^{(r)'} + 2 m_m \int_0^{L_{mi}} Y_{ci}^{(r)*} Y_{mi}^{(r)} dx_m + (-1)^{(i+1)} m_m L_{mi}^2 Y_{ci}^{(r)*} Y_{ci}^{(r)'} \\ & \left. + (-1)^{(i+1)} 2 m_i L_{mi} Y_{ci}^{(r)'} Y_{mi}^{(r)*} + (-1)^{(i+1)} 2 I_i Y_{ci}^{(r)'} Y_{mi}^{(r)'} + (-1)^{(i+1)} 2 m_m \int_0^{L_{mi}} Y_{ci}^{(r)'} Y_{mi}^{(r)} dx_m \right\} \end{aligned} \quad (25)$$

where

$$K_{rr} = \sum_{i=1}^2 \left\{ \int_0^{L_{ci}} \left[E_c I_c Y_{ci}^{(r)2''} - T Y_{ci}^{(r)2'} \right] dx + E_m I_m \int_0^{L_{mi}} Y_{mi}^{(r)2''} dx \right\} \quad (26)$$

$$[\omega_r]^2 = [K_{rr}] [M_{rr}]^{-1} \quad (28)$$

The conductor damping ratio (ζ) is introduced into Eq. (21) to obtain

$$\{\ddot{q}_r\} + [\omega_r]^2 \{q_r\} + 2\zeta[\omega_r] \{\dot{q}_r\} = [F_r] \quad (27)$$

5 Experiments

The experimental setup is depicted in Fig. 3 and the experiment was performed according to IEEE guide on conductor self-damping measurements [15]. The experiments were carried out on a 27.25 m test-span. The conductor (DRAKE 795 kcmil) was

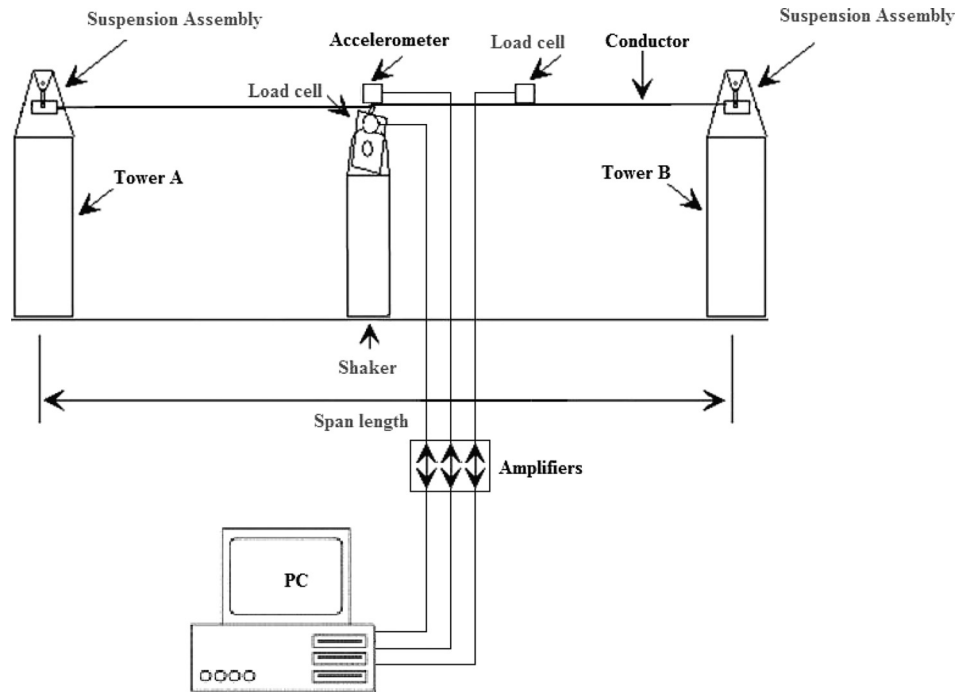


Fig. 3 Schematic of experimental setup

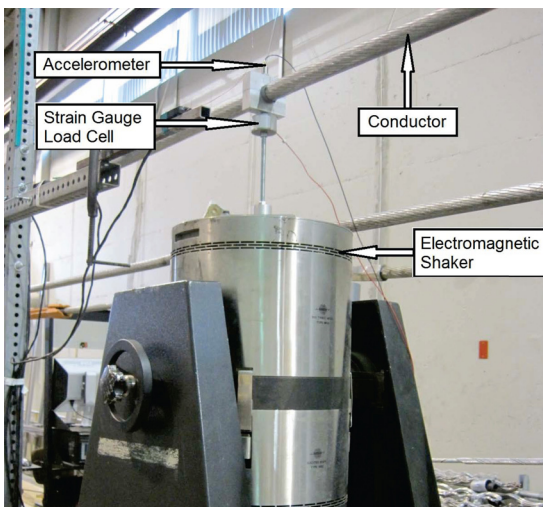


Fig. 4 Photograph of the conductor, shaker, load cell, and accelerometer

strung between two abutments made of steel reinforced concrete. A hydraulic Ram (cylinder) was installed at one end of the test-span to string the conductor at a desired tension (20% rated tensile strength (RTS) and 25% RTS). A cantilever weight (pulley system) was used at the other end of the test-span to maintain a constant tension throughout the span.

One load cell (1020 AF-50 kN-B) was placed at the end with the cantilever weight to monitor the tensile load. The other load cell (Dytran106V1) was used along with an accelerometer (B&K 4382) to measure the input force from the shaker and the midspan displacement of the conductor, respectively, as depicted in Fig. 4. The shaker (B&K 4802) was placed at midspan. Another accelerometer (B&K 4384) was placed at an antinode of the corresponding forcing frequency to measure the vibration displacement. The conductor was then vibrated at various frequencies and power levels based on the ALCOA wind power curve derived from wind tunnel tests on flexible cable [16]. The voltage signal from the

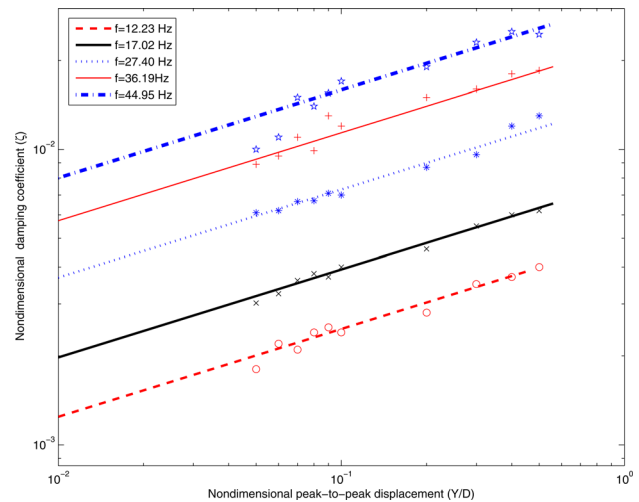


Fig. 5 Conductor damping constant for fixed frequency for $T = 20\%$ RTS

load cell and accelerometer were sent through charge amplifiers (Dytran415 and B&K 2635) by means of coaxial cable and then to a digital data acquisition system (PCI-6034E) for recording.

The recorded frequencies, force, displacements, and phase between the force and the displacement were employed in Eq. (29) to obtain the nondimensional damping ratio of the conductor, ζ . This is written as

$$\zeta = \frac{F y_f \sin \theta_d}{m L \omega_s^2 y_0} \quad (29)$$

where F is the driving force from the shaker, y_f is the displacement of the conductor at the shaker location (0 to peak), θ_d is phase angle between displacement and driving force, y_0 denotes the antinode vibration amplitude, and ω_s is the corresponding resonant circular frequency.

In agreement with Ref. [17], the recorded data herein indicate that the damping ratio is significantly dependent on the excitation

Table 1 Conductor and damper parameters

Parameter	
h	0.05 m
EI_c	1602 N m ²
m_c	1.628 kg/m
D_c	28.143 mm
RTS	139.2 kN
m_1	3.4 kg
m_2	1.46 kg
I_1	0.0175 kg m ²
I_2	0.015 kg m ²
$E_m I_m$	31.8 N m ²
L_{m1}	0.3 m
L_{m2}	0.22 m
m_m	0.25 kg/m

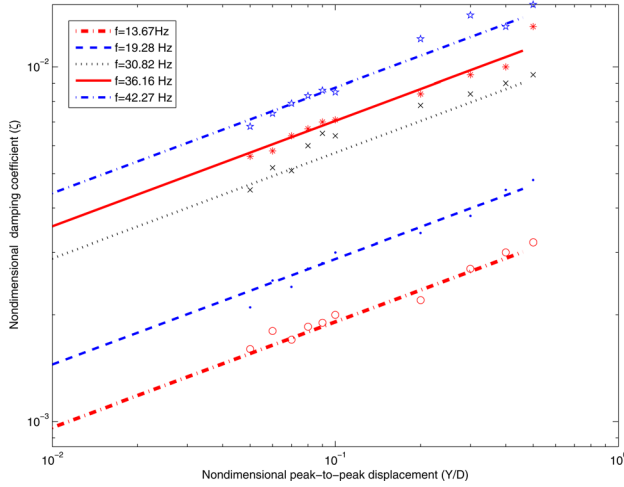


Fig. 6 Conductor damping constant for fixed frequency for $T = 25\%$ RTS

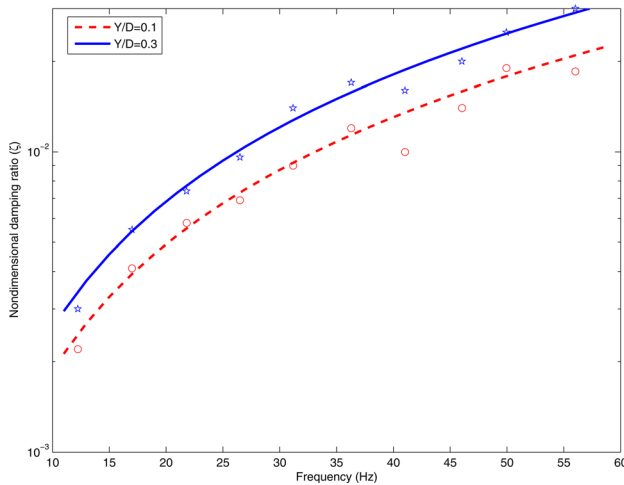


Fig. 7 Conductor damping constant for a fixed vibration amplitude for $T = 20\%$ RTS

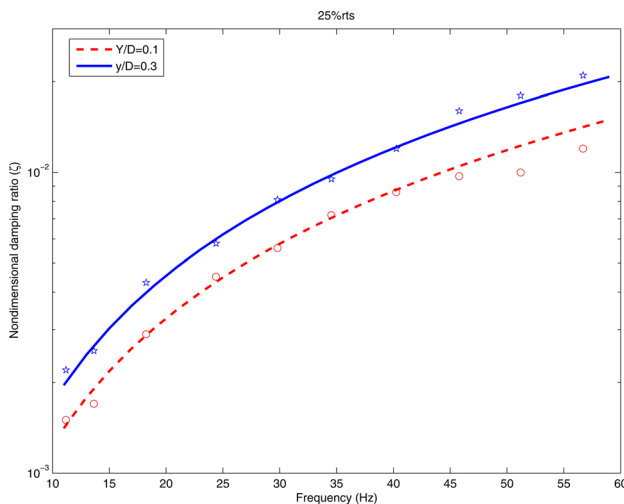


Fig. 8 Conductor damping constant for fixed vibration amplitude for $T = 25\%$ RTS

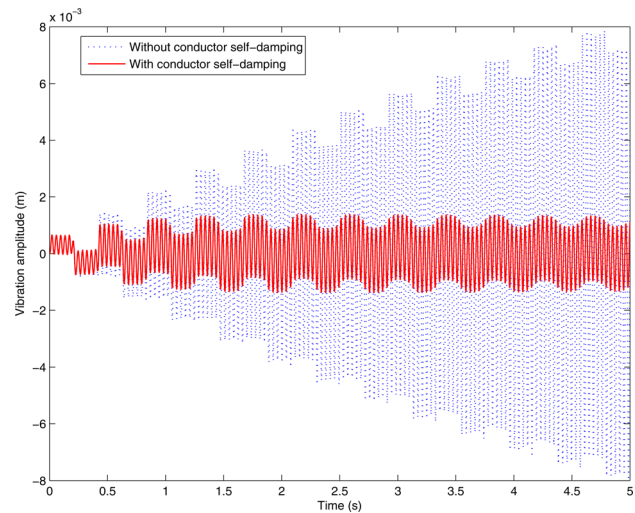


Fig. 9 Vibration response of the conductor with and without self-damping for $F_0 = 22.5$ N, $f = 26.5$ Hz, and $\zeta = 0.006$

frequency, vibration displacement, and the conductor tension. Hence the damping ratio can also be expressed as

$$\zeta = \frac{Cf^\alpha Y^\beta}{T^\gamma} \quad (30)$$

where f is the excitation frequency in Hz; Y is nondimensional peak to peak displacement (nondimensional with respect to the conductor diameter); T is the conductor tension; and C , α , β , and γ are constant. The constants— $C = 20760$, $\alpha = 1.406$, $\beta = 0.298$, and $\gamma = 1.835$ —were obtained using linear regression analysis:

In Figs. 5 and 6, the damping ratio is plotted against the nondimensional peak-to-peak amplitude for $T = 20\%$ RTS and $T = 25\%$ RTS, respectively. A line of best fit is plotted for every resonant frequency. Both figures show similar trends in that the damping ratio increases with increasing displacement. However, the damping ratio values for $T = 20\%$ RTS (Fig. 5) are higher than those for $T = 25\%$ RTS (Fig. 6). This implies that increasing the tension reduces the self-damping of the conductor.

For given displacements of $Y = 0.1$ and $Y = 0.3$, plots of damping ratio against resonant frequencies are depicted in Figs. 7 and 8 for $T = 20\%$ RTS and $T = 25\%$ RTS, respectively. These figures indicate that the conductor self-damping increases with increasing frequency. The figure with the lower tension (i.e., Fig. 7) exhibits higher conductor self-damping.

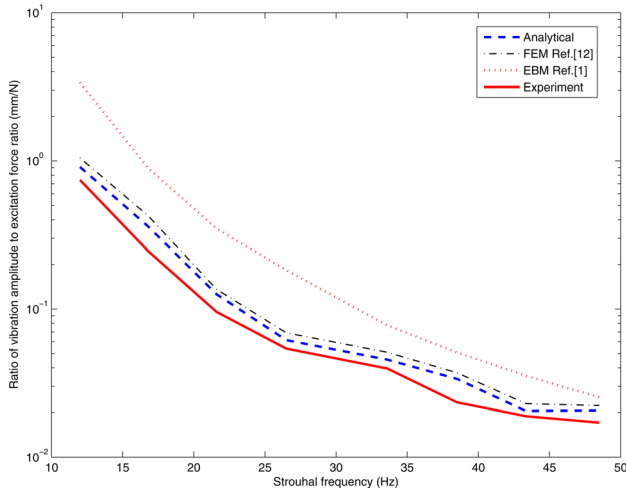


Fig. 10 Validation for the bare conductor

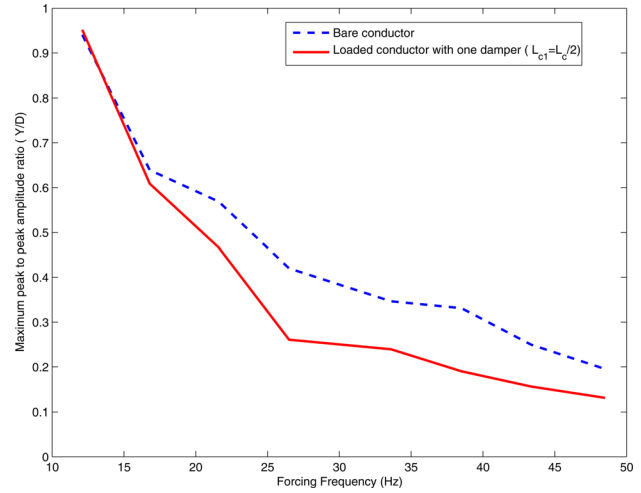


Fig. 13 Vibration response of a typical span length of transmission line with and without a damper

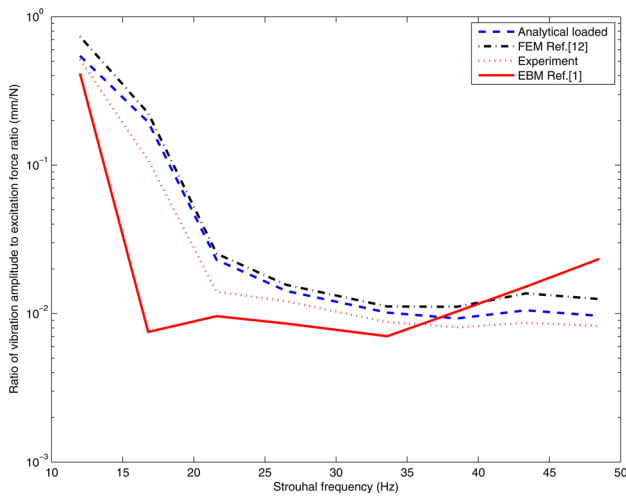


Fig. 11 Validation for the loaded conductor ($L_d = \frac{L_c}{2}$)

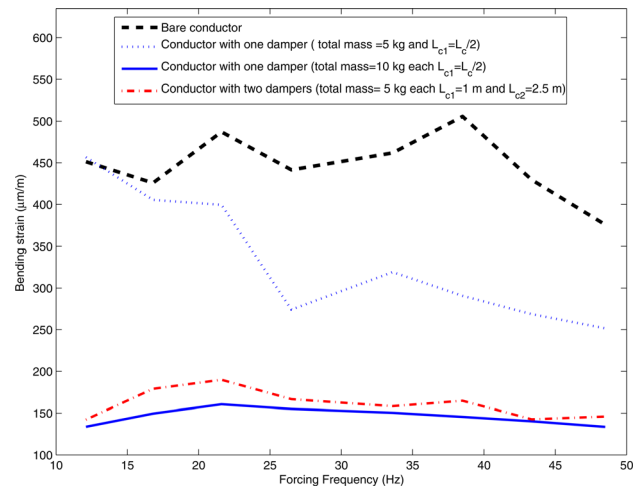


Fig. 14 Bending strain of a typical span length of transmission line with and without dampers

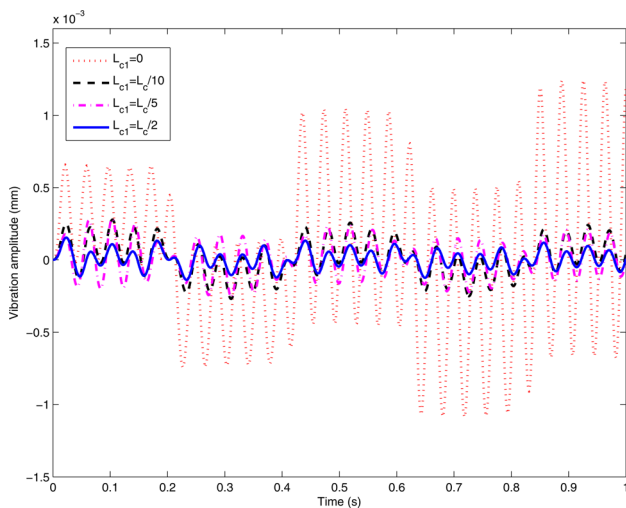


Fig. 12 Effect of damper location for $F_0 = 22.5 \text{ N}$, $f = 26.5 \text{ Hz}$, and $\zeta = 0.006$

6 Numerical Simulation

The numerical simulation is based on the tested conductor and Stockbridge damper. The material and geometry properties are listed in Table 1. The conductor tension was taken to be 20% RTS (27840 N). The time response of the bare conductor with and without self-damping is depicted in Fig. 9. The damping coefficient of the conductor was obtained by curve fitting the experimental data. It is observed that the vibration amplitude of the conductor without self-damping can be up to eight times higher than that with conductor self-damping. This implies that ignoring conductor self-damping can lead to erroneous prediction of the response of the conductor. Hence, the damping coefficient of the conductor is included in subsequent numerical simulations.

In Figs. 10 and 11, the validity of the present analytical model is examined using the experimental results. The former figure is the frequency response curve of the bare conductor, while the latter depicts the frequency response curve of the conductor with a Stockbridge damper located at $L_d = 0.94 \text{ m}$. Both figures show good agreement between the analytical and experimental results. The present analytical results are also compared to the FEM results used of Ref. [13] and the results obtained using the EBM employed in Ref. [1]. The comparisons indicate that the present analytical results agree best with the experiments.

It is observed from Fig. 10 that the energy balance method overestimates the response of the bare conductor, while Fig. 11 indicates that it underestimates the response of the loaded conductor. The plots in Figs. 10 and 11 also show that the ratio of the vibration amplitude to the excitation force significantly decreases with increasing frequency. However, the vibration response of the conductor with attached Stockbridge damper is much lower than that of the bare conductor.

For an excitation frequency of $f=26.5$ Hz, Fig. 12 shows the time response curve of the conductor for various dampers' location. The vibration amplitude is significantly reduced by attaching a Stockbridge damper at midspan.

A span length of $L_c = 366$ m is selected for the next numerical example. This selection ensures that the ratio of the conductor sag to span length is typical of existing transmission lines (i.e., 0.03). The equivalent wind force $F_0 = 370.9$ N.

Figure 13 presents the nondimensional response of the conductor (nondimensionalized with respect to conductor diameter) with and without damper for various forcing frequencies. It is observed that the conductor response reduces when the Stockbridge damper is attached except for $f=12.19$ Hz (corresponding to the 68th mode) which shows a slight increase in the conductor response. The reason for this increase is because the location of the damper for this specific frequency corresponds to a node.

The severity of Aeolian vibration is often measured by the bending strain ($\epsilon = \pi DYf \sqrt{(m/T)}$), which is used to examine the tendency of the conductor to experience fatigue failure. The bending strain is plotted against the forcing frequency in Fig. 14 for various dampers' total mass and location. Guided by suggested safe bending strain of $200 \mu(m/m)$ in the literature [1], it is evident that the calculated bending strain exceeds the strain limit for a bare conductor and that of a conductor with one damper attached with a total mass of 5 kg. When one damper with a total mass of 10 kg is attached or when two dampers, each with a total mass of 5 kg, are attached, the bending strain of the conductor is below the safe limit. Another important observation from Fig. 14 is that the bending strain of a conductor with one damper of a total mass of 10 kg attached at midspan is less than that observed with two attached dampers, each with a total mass of 5 kg.

7 Conclusion

An analytical model of a single conductor transmission line carrying a Stockbridge damper is developed. The model accounts for the conductor self-damping and the two-way coupling between the conductor and the damper. Experiments are conducted to validate the analytical model. Experimental data are employed along with linear regression analysis to obtain an explicit expression for the damping coefficient of the conductor. This expression is dependent on the frequency, tension, and vibration amplitude. Numerical examples show that the experimental results agree better with the proposed analytical model than the finite element and energy balance methods found in the literature. The results of the numerical analysis also indicate that the response of the conductor decreases significantly with increasing frequency. It is also observed that the attachment of the Stockbridge damper significantly reduces the vibration response of the conductor. The degree of reduction is dependent on the location and the mass of the Stockbridge damper.

Acknowledgment

The financial assistance from Hydro One, Inc., ON, Canada, is acknowledged. The authors are also grateful to Mr. Andrew Rizzetto and Mr. Dmitry Ladin of Kinectrics, Inc., Toronto, Canada, for their assistance with the experiments.

Appendix

For the sake of simplicity, the following notations are used:

$$\begin{aligned} s_i &= \sin \alpha L_{c_i}, & sh_i &= \sinh \beta L_{c_i}, \\ c_i &= \cos \alpha L_{c_i}, & ch_i &= \cosh \beta L_{c_i}, \\ s_{\Omega_i} &= \sin \Omega_m L_{m_i}, & sh_{\Omega_i} &= \sinh \Omega_m L_{m_i}, \\ c_{\Omega_i} &= \cos \Omega_m L_{m_i}, & ch_{\Omega_i} &= \cosh \Omega_m L_{m_i} \end{aligned}$$

$$\text{where } \alpha = \sqrt{-\frac{S^2}{2} + \sqrt{\frac{S^4}{4} + \Omega_c^4}} \text{ and } \beta = \sqrt{\frac{S^2}{2} + \sqrt{\frac{S^4}{4} + \Omega_c^4}}.$$

$$\Omega_c = (\omega^2 m_c / E_c I_c)^{1/4}, \Omega_m = (\omega^2 m_m / E_m I_m)^{1/4}, \text{ and } S = \sqrt{T / E_c I_c}.$$

By ignoring the hyperbolic function terms since the tension and the span length in transmission lines are usually very high, the conductor mode shapes for each segment can be expressed as Ref. [14]

$$Y_{c_1}(x) = \sin \alpha x_1 \quad (A1)$$

$$Y_{c_2}(x) = \frac{s_1}{s_2} \sin \alpha x_2 \quad (A2)$$

The mode shapes of the messenger is expressed as

$$\begin{aligned} Y_{m_i}(x_m) &= B_{1i} \sin \Omega_m x_m + B_{2i} \cos \Omega_m x_m + B_{3i} \sinh \Omega_m x_m \\ &+ B_{4i} \cosh \Omega_m x_m - (Y_{c_1}^* + (-1)^{(i+1)} x_m Y_{c_1}^*) \end{aligned} \quad (A3)$$

where the constant of integration are given as

$$\begin{aligned} B_{1i} &= \frac{1}{\lambda_i} \{ \mathcal{F}_{11,1} \mathcal{F}_{(i+4),7} \mathcal{F}_{(i+6),8} - \mathcal{F}_{11,1} \mathcal{F}_{(i+4),7} \mathcal{F}_{(i+6),6} \\ &+ \mathcal{F}_{1,1} \mathcal{F}_{(i+4),6} \mathcal{F}_{(i+6),8} - \mathcal{F}_{1,1} \mathcal{F}_{(i+4),8} \mathcal{F}_{(i+6),6} \\ &- \mathcal{F}_{11,1} \mathcal{F}_{(i+4),8} \mathcal{F}_{(i+6),7} + \mathcal{F}_{11,1} \mathcal{F}_{(i+4),6} \mathcal{F}_{(i+6),7} \} \end{aligned} \quad (A4)$$

$$\begin{aligned} B_{2i} &= -\frac{1}{\lambda_i} \{ -\mathcal{F}_{1,1} \mathcal{F}_{(i+6),8} \mathcal{F}_{(i+4),7} + \mathcal{F}_{1,1} \mathcal{F}_{(i+6),8} \mathcal{F}_{(i+4),5} \\ &+ \mathcal{F}_{1,1} \mathcal{F}_{(i+6),7} \mathcal{F}_{(i+4),8} - \mathcal{F}_{1,1} \mathcal{F}_{(i+6),5} \mathcal{F}_{(i+4),8} \\ &- \mathcal{F}_{11,1} \mathcal{F}_{(i+6),5} \mathcal{F}_{(i+4),7} + \mathcal{F}_{11,1} \mathcal{F}_{(i+6),7} \mathcal{F}_{(i+4),5} \} \end{aligned} \quad (A5)$$

$$\begin{aligned} B_{3i} &= -\frac{1}{\lambda_i} \{ \mathcal{F}_{11,1} \mathcal{F}_{(i+6),8} \mathcal{F}_{(i+4),5} - \mathcal{F}_{11,1} \mathcal{F}_{(i+6),6} \mathcal{F}_{(i+4),5} \\ &+ \mathcal{F}_{1,1} \mathcal{F}_{(i+4),6} \mathcal{F}_{(i+6),8} - \mathcal{F}_{1,1} \mathcal{F}_{(i+4),8} \mathcal{F}_{(i+6),6} \\ &- \mathcal{F}_{11,1} \mathcal{F}_{(i+6),5} \mathcal{F}_{(i+4),8} + \mathcal{F}_{11,1} \mathcal{F}_{(i+6),5} \mathcal{F}_{(i+4),6} \} \end{aligned} \quad (A6)$$

$$\begin{aligned} B_{4i} &= \frac{1}{\lambda_i} \{ -\mathcal{F}_{11,1} \mathcal{F}_{(i+6),5} \mathcal{F}_{(i+4),7} - \mathcal{F}_{1,1} \mathcal{F}_{(i+6),6} \mathcal{F}_{(i+4),7} \\ &+ \mathcal{F}_{1,1} \mathcal{F}_{(i+6),6} \mathcal{F}_{(i+4),5} + \mathcal{F}_{11,1} \mathcal{F}_{(i+6),7} \mathcal{F}_{(i+4),5} \\ &+ \mathcal{F}_{1,1} \mathcal{F}_{(i+6),7} \mathcal{F}_{(i+4),6} - \mathcal{F}_{1,1} \mathcal{F}_{(i+6),5} \mathcal{F}_{(i+4),6} \} \end{aligned} \quad (A7)$$

where

$$\begin{aligned} \lambda_i &= \mathcal{F}_{(i+6),8} \mathcal{F}_{(i+4),7} - \mathcal{F}_{(i+6),8} \mathcal{F}_{(i+4),5} - \mathcal{F}_{(i+6),6} \mathcal{F}_{(i+4),8} \\ &+ \mathcal{F}_{(i+6),8} \mathcal{F}_{(i+4),5} \\ &- \mathcal{F}_{(i+6),7} \mathcal{F}_{(i+4),8} + \mathcal{F}_{(i+6),7} \mathcal{F}_{(i+4),6} + \mathcal{F}_{(i+6),5} \mathcal{F}_{(i+4),8} \\ &- \mathcal{F}_{(i+6),5} \mathcal{F}_{(i+4),6} \end{aligned}$$

and

$$\mathcal{F}_{1,1} = s_1, \mathcal{F}_{1,2} = sh_1, \mathcal{F}_{1,3} = -s_2, \mathcal{F}_{1,4} = -sh_2$$

$$\mathcal{F}_{2,1} = \alpha c_1, \mathcal{F}_{2,2} = \beta ch_1, \mathcal{F}_{2,3} = \alpha c_2, \mathcal{F}_{2,4} = \beta ch_2$$

$$\mathcal{F}_{3,1} = \alpha c_1 h^2 (m_1 + m_2 + m_{m_1} + m_{m_2}) + \frac{\alpha^2}{\omega^2} E_c I_c s_1$$

$$\mathcal{F}_{3,2} = \beta ch_1 h^2 (m_1 + m_2 + m_{m_1} + m_{m_2}) - \frac{\beta^2}{\omega^2} E_c I_c sh_1$$

$$\mathcal{F}_{3,3} = -\frac{\alpha^2}{\omega^2} s_2 E_c I_c, \mathcal{F}_{3,4} = \frac{\beta^2}{\omega^2} sh_2 E_c I_c$$

$$\begin{aligned}
F_{3,5} &= m_1 L_{m_1} s_{\Omega_1} + \Omega_m c_{\Omega_1} I_1 + m_m \left(-\frac{L_{m_1} c_{\Omega_1}}{\Omega_m} + \frac{1}{\Omega_m^2} s_{\Omega_1} \right) \\
F_{3,6} &= m_1 L_{m_1} c_{\Omega_1} - \Omega_m s_{\Omega_1} I_1 + m_m \left(\frac{L_{m_1} s_{\Omega_1}}{\Omega_m} + \frac{1}{\Omega_m^2} (c_{\Omega_1} - 1) \right) \\
F_{3,7} &= m_1 L_{m_1} s h_{\Omega_1} + \Omega_m c h_{\Omega_1} I_1 + m_m \left(\frac{L_{m_1} c h_{\Omega_1}}{\Omega_m} - \frac{1}{\Omega_m^2} s h_{\Omega_1} \right) \\
F_{3,8} &= m_1 L_{m_1} c h_{\Omega_1} + \Omega_m s h_{\Omega_1} I_1 + m_m \left(\frac{L_{m_1} s h_{\Omega_1}}{\Omega_m} - \frac{1}{\Omega_m^2} (c h_{\Omega_1} - 1) \right) \\
F_{3,9} &= -m_2 L_{m_2} s_{\Omega_2} - \Omega_m c_{\Omega_2} I_2 - m_m \left(-\frac{L_{m_2} c_{\Omega_2}}{\Omega_m} + \frac{1}{\Omega_m^2} s_{\Omega_2} \right) \\
F_{3,10} &= -m_2 L_{m_2} c_{\Omega_2} + \Omega_m s_{\Omega_2} I_2 - m_m \left(\frac{L_{m_2} s_{\Omega_2}}{\Omega_m} + \frac{1}{\Omega_m^2} (c_{\Omega_2} - 1) \right) \\
F_{3,11} &= -m_2 L_{m_2} s h_{\Omega_2} - \Omega_m c h_{\Omega_2} I_2 - m_m \left(\frac{L_{m_2} c h_{\Omega_2}}{\Omega_m} - \frac{1}{\Omega_m^2} s h_{\Omega_2} \right) \\
F_{3,12} &= -m_2 L_{m_2} c h_{\Omega_2} - \Omega_m s h_{\Omega_2} I_2 - m_m \left(\frac{L_{m_2} s h_{\Omega_2}}{\Omega_m} - \frac{1}{\Omega_m^2} (c h_{\Omega_2} - 1) \right) \\
F_{4,1} &= \frac{-\alpha^3}{\omega^2} c_1 E_c I_c, \quad F_{4,2} = \frac{\beta^3}{\omega^2} c h_1 E_c I_c \\
F_{4,3} &= \frac{-\alpha^3}{\omega^2} c_2 E_c I_c, \quad F_{4,4} = \frac{\beta^3}{\omega^2} c h_2 E_c I_c \\
F_{4,5} &= m_1 s_{\Omega_1} - \frac{m_m}{\Omega_m} (c_{\Omega_1} - 1), \quad F_{4,6} = m_1 c_{\Omega_1} + \frac{m_m}{\Omega_m} s_{\Omega_1} \\
F_{4,7} &= m_1 s h_{\Omega_1} + \frac{m_m}{\Omega_m} (c h_{\Omega_1} - 1), \quad F_{4,8} = m_1 c h_{\Omega_1} + \frac{m_m}{\Omega_m} s h_{\Omega_1} \\
F_{4,9} &= m_2 s_{\Omega_2} - \frac{m_m}{\Omega_m} (c_{\Omega_2} - 1), \quad F_{4,10} = m_2 c_{\Omega_2} + \frac{m_m}{\Omega_m} s_{\Omega_2} \\
F_{4,11} &= m_2 s h_{\Omega_2} + \frac{m_m}{\Omega_m} (c h_{\Omega_2} - 1), \quad F_{4,12} = m_2 c h_{\Omega_2} + \frac{m_m}{\Omega_m} s h_{\Omega_2} \\
F_{5,5} &= s_{\Omega_1} - \lambda_{m_1} \Omega_m^3 c_{\Omega_1}, \quad F_{5,6} = c_{\Omega_1} + \lambda_{m_1} \Omega_m^3 s_{\Omega_1} \\
F_{5,7} &= s h_{\Omega_1} + \lambda_{m_1} \Omega_m^3 c h_{\Omega_1}, \quad F_{5,8} = c h_{\Omega_1} + \lambda_{m_1} \Omega_m^3 s h_{\Omega_1} \\
F_{6,9} &= s_{\Omega_2} - \lambda_{m_2} \Omega_m^3 c_{\Omega_2}, \quad F_{6,10} = c_{\Omega_2} + \lambda_{m_2} \Omega_m^3 s_{\Omega_2} \\
F_{6,11} &= s h_{\Omega_2} + \lambda_{m_2} \Omega_m^3 c h_{\Omega_2}, \quad F_{6,12} = c h_{\Omega_2} + \lambda_{m_2} \Omega_m^3 s h_{\Omega_2} \\
F_{7,5} &= c_{\Omega_1} + \kappa_{m_1} \Omega_m s_{\Omega_1}, \quad F_{7,6} = -s_{\Omega_1} + \kappa_{m_1} \Omega_m c_{\Omega_1} \\
F_{7,7} &= c h_{\Omega_1} - \kappa_{m_1} \Omega_m s h_{\Omega_1}, \quad F_{7,8} = s h_{\Omega_1} - \kappa_{m_1} \Omega_m c h_{\Omega_1} \\
F_{8,9} &= c_{\Omega_2} + \kappa_{m_2} \Omega_m s_{\Omega_2}, \quad F_{8,10} = -s_{\Omega_2} + \kappa_{m_2} \Omega_m c_{\Omega_2} \\
F_{8,11} &= c h_{\Omega_2} - \kappa_{m_2} \Omega_m s h_{\Omega_2}, \quad F_{8,12} = s h_{\Omega_2} - \kappa_{m_2} \Omega_m c h_{\Omega_2}
\end{aligned}$$

$$\begin{aligned}
\mathcal{F}_{9,1} &= \mathcal{F}_{10,1} = -s_1, \quad \mathcal{F}_{9,2} = \mathcal{F}_{10,2} = -s h_1 \\
\mathcal{F}_{9,6} &= \mathcal{F}_{9,8} = \mathcal{F}_{10,10} = \mathcal{F}_{10,12} = 1 \\
\mathcal{F}_{11,1} &= \frac{-\alpha c_1}{\Omega_m}, \quad \mathcal{F}_{11,2} = \frac{-\beta c h_1}{\Omega_m} \\
\mathcal{F}_{12,1} &= -\mathcal{F}_{11,1}, \quad \mathcal{F}_{12,2} = -\mathcal{F}_{11,2}
\end{aligned}$$

References

- [1] Lu, M. L., and Chan, J. K., 2007, "An Efficient Algorithm for Aeolian Vibration of Single Conductor With Multiple Dampers," *IEEE Trans. Power Delivery*, **22**(3), pp. 1822–1829.
- [2] Claren, R., and Diana, G., 1969, "Mathematical Analysis of Transmission Line Vibration," *IEEE Trans. Power Delivery*, **60**(2), pp. 1741–1771.
- [3] Kraus, M., and Hagedorn, P., 1991, "Aeolian Vibration: Wind Energy Input Evaluated From Measurements on an Energized Transmission Lines," *IEEE Trans. Power Delivery*, **6**(3), pp. 1264–1270.
- [4] Verma, H., and Hagedorn, P., 2004, "Wind Induced Vibration of Long Electrical Overhead Transmission Line Spans: A Modified Approach," *J. Wind Struct.*, **8**(2), pp. 89–106.
- [5] Tompkins, J. S., Merrill, L. L., and Jones, B. L., 1956, "Quantitative Relationships in Conductor Vibration Using Rigid Models" *IEEE Trans. Power Apparatus Syst.*, **75**(11), pp. 879–894.
- [6] Rawlins, C. B., 1958, "Recent Developments in Conductor Vibration," Alcoa Technical Paper No. 13, 1958.
- [7] Nigol, O., and Houston, H. J., 1985, "Aeolian Vibration of Single Conductor and Its Control," *IEEE Trans. Power Delivery*, **104**(11), pp. 3245–3254.
- [8] Hardy, C., and Noiseux, D. U., 1996, *Modeling of a Single Conductor-Damper System Response, Vol 1: Theoretical and Validation Manual*, CEA, Hydro, QC, Montreal, Canada.
- [9] Noiseux, D. U., Hardy, C., and Houle, S., 1987, "Statistical Methods Applied to Aeolian Vibration of Overhead Conductors," *J. Sound Vib.*, **113**(2), pp. 245–255.
- [10] Tsui, Y. T., 1982, "Recent Advances in Engineering Science as Applied to Aeolian Vibrations an Alternative Approach," *Electr. Power Res.*, **5**, pp. 73–85.
- [11] Gonçalves, R. T., Rosetti, G. F., Fajarra, A. L. C., Franzini, G. R., Freire, C. M., and Meneghini, J. R., 2012, "Experimental Comparison of Two Degrees-of-Freedom Vortex-Induced Vibration on High and Low Aspect Ratio Cylinders With Small Mass Ratio," *ASME J. Vib. Acoust.*, **134**, p. 0161009.
- [12] Barry, O., Oguamanam, D. C. D., and Lin, D. C., 2010, "Free Vibration Analysis of a Single Conductor With a Stockbridge Damper," 23rd Canadian Congress of Applied Mechanics (CANCAM 2011), Vancouver, Canada, June 5–9, pp. 944–946.
- [13] Barry, O., Oguamanam, D. C. D., and Lin, D. C., 2013, "Aeolian Vibration of a Single Conductor With a Stockbridge Damper," *IMechE: Part C, J. Mech. Eng. Sci.*, **227**(5), pp. 935–945.
- [14] Barry, O., Zu, J. W., and Oguamanam, D. C. D., 2014, "Analytical and Experimental Investigation of Overhead Transmission Line Vibration," *J. Vib. Control* (in press).
- [15] IEEE Power & Energy Society, 1978, "IEEE Guide on Conductor Self-Damping Measurements," Institute of Electrical and Electronics Engineers, New York, *IEEE Standard No. 563–1978*.
- [16] Rawlins, C. B., 1982 "Power Imparted by Wind to a Model of a Vibrating Conductor," ALCOA Laboratories, Massena, NY, Report No. 93-82-1.
- [17] Diana, G., Falco, M., and Manenti, A., 2000, "On the Measurement of Overhead Transmission Lines Conductor Self-Damping," *IEEE Trans. Power Delivery*, **15**(1), pp. 285–292.